Nuclear Engineering and Design 240 (2010) 656–667

Contents lists available at ScienceDirect

Nuclear Engineering and Design

journal homepage: www.elsevier.com/locate/nucengdes

Thermal-hydraulic and aerosol containment phenomena modelling in ASTEC severe accident computer code

Ivo Kljenak[a,*], Maik Dapper[b], Jiří Dienstbier[c], Luis E. Herranz[d], Marco K. Koch[b], Joan Fontanet[d]

[a] Jožef Stefan Institute, Jamova cesta 39, SI-1000 Ljubljana, Slovenia
[b] Ruhr-Universität Bochum, Institute for Energy Systems and Energy Economics, Germany
[c] Nuclear Research Institute Řež, Czech Republic
[d] Centro de Investigaciones Energeticas Medio Ambientales y Tecnologicas, Madrid, Spain

ARTICLE INFO

Article history:
Received 20 March 2009
Received in revised form
13 November 2009
Accepted 3 December 2009

ABSTRACT

Transients in containment systems of different scales (Phebus.FP containment, KAEVER vessel, Battelle Model Containment, LACE vessel and VVER-1000 nuclear power plant containment) involving thermal-hydraulic phenomena and aerosol behaviour, were simulated with the computer integral code ASTEC. The results of the simulations in the first four facilities were compared with experimental results, whereas the results of the simulated accident in the VVER-1000 containment were compared to results obtained with the MELCOR code. The main purpose of the simulations was the validation of the CPA module of the ASTEC code. The calculated results support the applicability of the code for predicting in-containment thermal-hydraulic and aerosol phenomena during a severe accident in a nuclear power plant.

1. Introduction

The accurate prediction of thermal-hydraulic phenomena and fission product behaviour in a nuclear power plant (NPP) containment during a hypothetical severe accident is an important part of safety analyses and plant licensing. Despite recent progress made in the modelling of containment phenomena using CFD (Computational Fluid Dynamics) codes, lumped-parameter codes are still the basic tools that are used for safety analyses of actual plants. The main reasons are the following:

– despite promising results, CFD codes have not yet been thoroughly validated, and their results are still uncertain;
– CFD codes necessitate relatively fine numerical grids, which makes simulations of phenomena in actual containments impractical.

Thus, the further development and validation of lumped-parameter containment codes, such as COCOSYS, CONTAIN, MELCOR (containment), and ASTEC (the module CPA – Containment Part of ASTEC) are still important for the near and mid-term future of the nuclear industry.

Within the Severe Accident Research Network of Excellence (SARNET), which was part of the 6th EU Framework Programme, activities on the validation of the European integral severe accident code ASTEC, which included validation of the CPA module, were carried out. The ASTEC code is being developed jointly by the Institut de Radioprotection et de Sûreté Nucléaire – IRSN (France) and the Gesellschaft für Anlagen und Reaktorsicherheit – GRS (Germany) (Klein-Hessling and Schwinges, 1998; Bestele and Klein-Hessling, 2000; Van Dorsselaere and Schwinges, 2006). Different versions of the ASTEC code (V1.2 and V1.3) were used, but the CPA module effectively differed mostly in some numerical improvements, and observed differences on the calculated results were negligible. The validation concerned the modelling of thermal-hydraulic phenomena as well as aerosol and fission products behaviour. For this purpose, simulations were carried out of transients in containment systems of different scales. The code was validated by comparing simulation results with experimental data, as well as with results obtained with other established severe accident codes that have been extensively validated. Although this last option cannot be considered as a genuine validation, a concordance of simulation results still supports the validity of the tested physical models.

In the present work, validation activities of the ASTEC (CPA) code that were carried out within SARNET are presented. Topics are limited to thermal-hydraulic and aerosol phenomena. Transients in experimental and real systems of different scale were simulated. The Phebus.FP containment vessel and the KAEVER vessel may be considered as small-scale experimental containment facilities, whereas the Battelle Model Containment and the LACE facility may be considered as large-scale facilities. Simulation results were compared with experimental data obtained in these facilities. To further validate the code in a real-scale system, a hypothetical accident scenario in a VVER-1000 NPP containment was simulated, and

* Corresponding author. Tel.: +386 1 5885332; fax: +386 1 5885377.
E-mail address: ivo.kljenak@ijs.si (I. Kljenak).

0029-5493/$ – see front matter © 2009 Elsevier B.V. All rights reserved.
doi:10.1016/j.nucengdes.2009.12.002

the results were compared to simulation results obtained with the severe accident MELCOR code. The comparison of results provides a general overview of the current abilities and drawbacks of the CPA module of the ASTEC code.

2. Facilities and experiments

2.1. Phebus facility and FPT2 test

The Phebus.FP experimental facility (IRSN, 2002) was operated by the Institut de Radioprotection et de Sûreté Nucléaire and located in Cadarache (France). It is volume scaled-down (1:5000) from a 900 MWe Pressurized Water Reactor (PWR) and consists of three main sections:

– core, where the fuel bundle is located,
– primary circuit, which includes mock-ups of circuit components like the steam generator,
– containment: a vessel which receives the material transported through the primary circuit.

The containment vessel has a 10 m^3 volume and consists of a 4.5 m high and 1.77 m diameter cylinder closed at the top and at the bottom by ellipsoidal surfaces (Fig. 1). The internal facing surfaces of the vessel are heated, so that steam condensation on them may be prevented by setting a sufficiently high temperature. Three cylindrical structures that are attached to the containment ceiling act as condensers. Each condenser has a dry (high temperature) and a wet (low temperature) part, on which steam condenses.

The objective of the test FPT2 was to analyze: the core degradation; the release of fission products, control and structural materials; their transport and retention in the circuit and the behaviour of the isotopes in the containment vessel. Specifically, the test addressed these issues under the following conditions (Ritter and Zabiego, 2002): irradiated fuel; a Ag–In–Cd control rod in the core; low pressure and weakly oxidizing environment in the test bundle and primary circuit; a weakly condensing atmosphere and alkaline sump in the containment. Measurements of thermal-hydraulic parameters were performed as well. The sump contained an initial water volume of 110 l. During the test, steam, hydrogen, nitrogen and helium entered the containment, and gas was removed for sampling (Fig. 2). The atmosphere of the containment vessel was well below saturation. At t = 24,240 s after the start of the test, the containment was isolated and the so-called “aerosol phase” started and lasted until t = 157,140 s. During this phase, the suspended particle concentration decreased for several orders of magnitude.

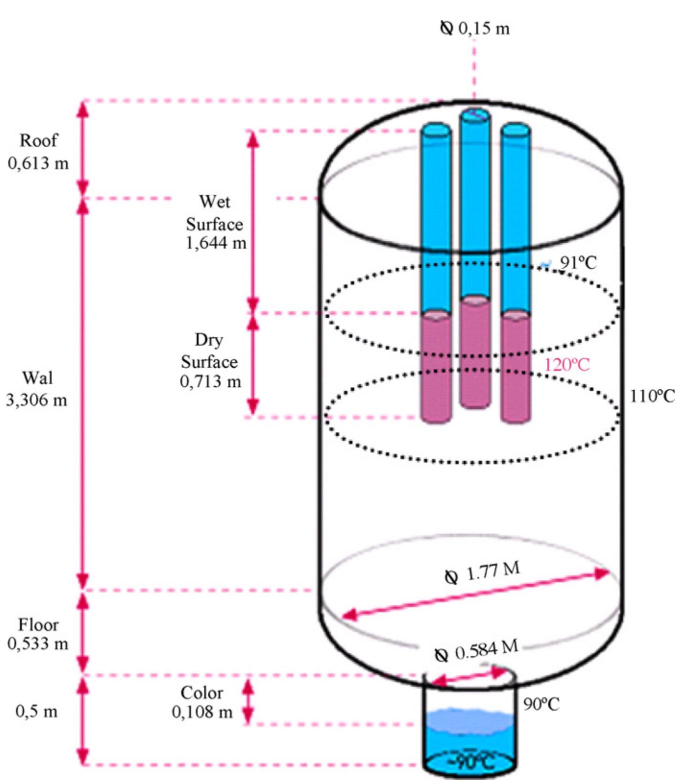

Fig. 1. Geometry and thermal conditions in Phebus containment vessel during test FPT2.

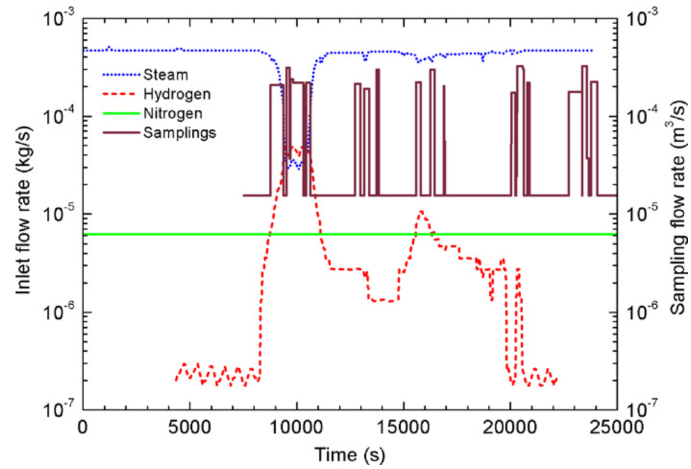

Fig. 2. Inlet and outlet gas mass flow rates in Phebus containment vessel during test FPT2.

2.2. KAEVER facility and experiments

The KAEVER experimental facility was located at Battelle Ingenieurtechnik (now Becker Technologies) in Eschborn (Germany). The purpose of the KAEVER experimental programme was the investigation of the deposition behaviour of core melting aerosols in a containment compartment (Firnhaber et al., 2002). The facility was a horizontal cylindrical steel vessel (inner free volume: 10.595 m^3) with plane faces and short rectangular doorways attached on both sides (Fig. 3). Some walls of the vessel were equipped with heater mats between the insulation and the inside steel. The condensate accumulated on the bottom of the cylindrical part. The thermal-hydraulic behaviour of the test vessel was determined by the electric heating, the injections, the heat losses and the leakage. Injections of steam and nitrogen (used as carrier gas for aerosols) were provided.

Four KAEVER experiments, during which the atmosphere was saturated, were simulated with the ASTEC code (Kljenak and Mavko, 2006a):

– K148: injection of Ag (non-soluble) aerosols,
– K188: injection of CsOH (soluble) aerosols,
– K186: injection of CsOH and Ag aerosols,
– K187: injection of CsOH, CsI (soluble) and Ag aerosols.

Each experiment consisted of two phases: a preconditioning phase and the execution of the experiment. During the preconditioning phase, quasi-stationary conditions in the test vessel were obtained by steam injection and electric heating. Steam injection was continued during the execution of the experiment. Aerosols were injected by turning on inductive heating of aerosol generators until the material was completely evaporated. Finally, the

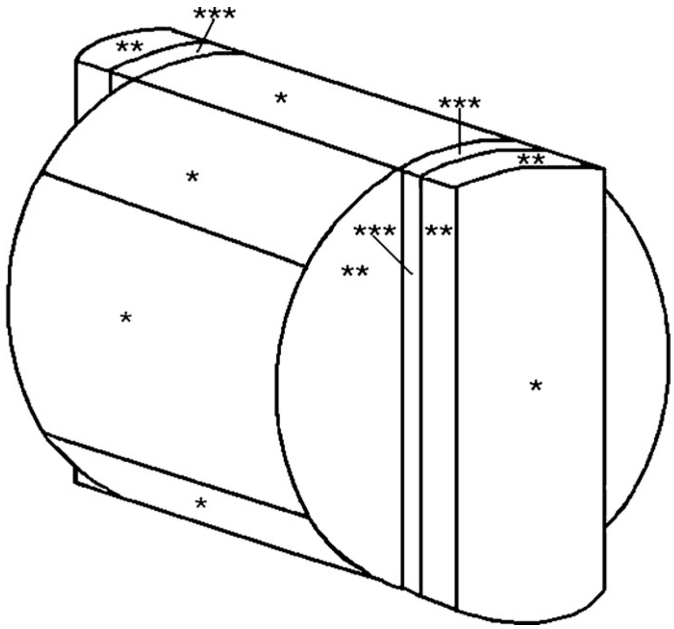

Fig. 3. Perspective view of KAEVER test vessel (*: heated walls; **: isolated walls; ***: non-isolated walls).

depletion of aerosols was observed without further change in the injection or boundary conditions. The experiments (from the end of the preconditioning phase) lasted between 24,000 s and 41,400 s.

2.3. Battelle Model Containment and PACOS Px1.2 experimental sequence

The Battelle Model Containment (BMC) was located at Battelle Ingenieurtechnik (Germany) and represented a linear 1:4 downsized model of a German PWR containment (Wilkening et al., 2007). The compartmentalized facility, which was built of unlined concrete, had a variable geometry and a total volume of about 640 m^3 (Fig. 4). In the PACOS Px1 experiment, the volume was reduced to 600 m^3, because the annulus room R7 was sealed. In the dome of the facility (room R9), a spray system with 32 nozzles in a flow ring pipe was installed. The steam injection was located in the inner room R3 (Kanzleiter et al., 1996).

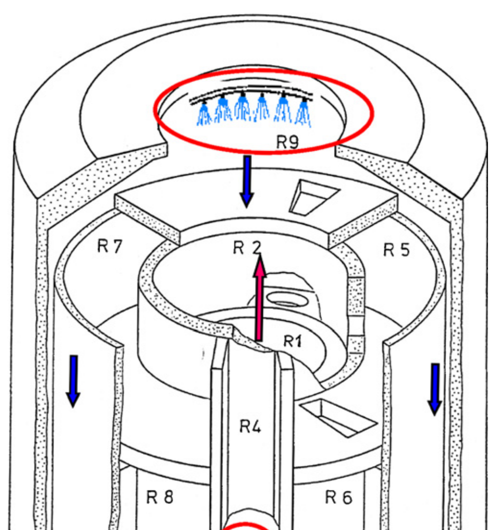

Fig. 4. Perspective view of Battelle Model Containment.

The objective of the considered sequence PACOS Px1.2 of the experiment PACOS Px1, which was simulated with the ASTEC code, was the analysis of steam-air mixing in the containment and of the influence of containment spray systems. During the first phase of the sequence Px1.2 (Fig. 5), the pressure decreased due to the abrupt actuation of the sprays, while the steam injection rate remained constant. During the second phase, the steam injection rate was increased by a factor of three with a continuous constant spray water mass flow rate, so that the pressure increased as a consequence. During the third phase, the pressure decreased as the spray mass flow rate was abruptly increased. In the last phase, the steam injection was stopped and the pressure subsequently decreased. The Px1.2 sequence lasted about 4300 s (Kanzleiter et al., 1996).

2.4. LACE vessel and LA4 experiment

The LACE (LWR Aerosol Containment Experiment) experimental facility was located at Westinghouse Hanford Company, USA (McCormack et al., 1987). The facility was a vertical cylindrical steel vessel, with an inner free volume of 852 m^3 (Fig. 6). The overall height of the vessel was 20.3 m, and the inner diameter of the cylindrical part was 7.62 m. The walls were not heated and were insulated on the outside. The heat structures consisted of the vessel walls and of internal steel structures.

The experiment LA4, which was simulated with the ASTEC code (Kljenak and Mavko, 2006b, 2007), consisted of the following phases:

1. Heatup: steam and nitrogen injection through aerosol delivery line – ADL (starting at $t = -3000$ s).
2. Injection of steam and CsOH (soluble) aerosols with carrier gas (from $t = 80$ s to $t = 1900$ s).
3. Injection of steam and CsOH and MnO (non-soluble) aerosols with carrier gas (until $t = 3200$ s).
4. Injection of steam and MnO aerosols with carrier gas (until $t = 4800$ s).
5. Steady state: steam and nitrogen injection through ADL (until $t = 16{,}800$ s).
6. Venting, with steam and nitrogen injection through ADL (until $t = 25{,}900$ s).
7. Cooldown: nitrogen injection through ADL and vent valve opened (at $t = 48{,}000$ s).

In addition, nitrogen was injected continuously to purge the instruments. A peculiar characteristic of the experiment LA4 was venting after the injection of aerosols, which was meant to simulate a delayed containment failure.

2.5. VVER-1000/320 NPP containment and ABH scenario

To assess the ASTEC code when simulating an accident scenario in an actual plant, a standard VVER-1000/320 containment was selected, based on the Balakovo NPP (Russian Federation). The ABH scenario (hot leg large break loss-of-coolant accident – LOCA – with blackout) was simulated from the initiation up to the vessel bottom head failure at 11,322 s. The initiating event is a double-ended break of one of four main circulation loops with loss of electric power, so that the emergency core cooling and spray systems are not actuated. Core uncovery is followed by oxidation, fission product gap release, core plate failing and failure of the vessel bottom head. Because the fluid source mass flow rate to the containment is very high during the first minute, followed later by a much lower

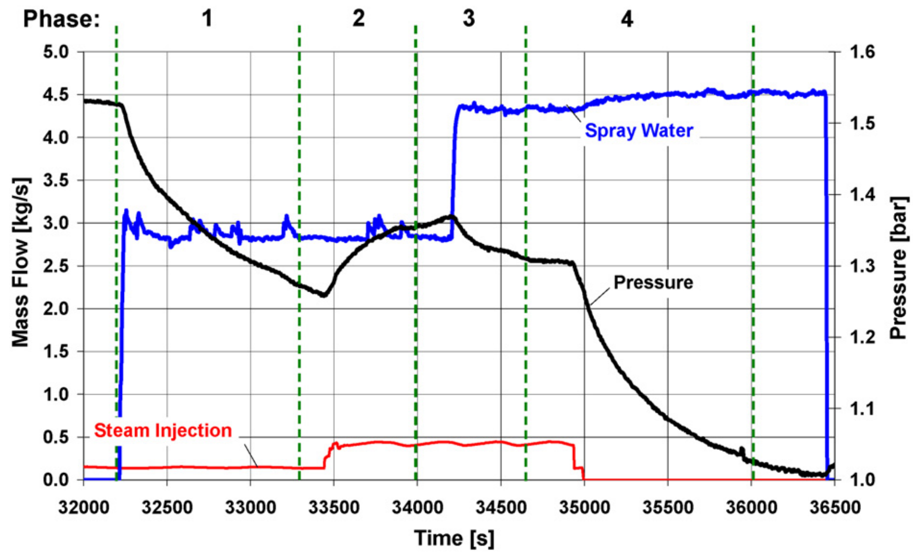

Fig. 5. Experimental injection mass flow rates and resulting pressure progression in BMC during PACOS Px1.2 sequence.

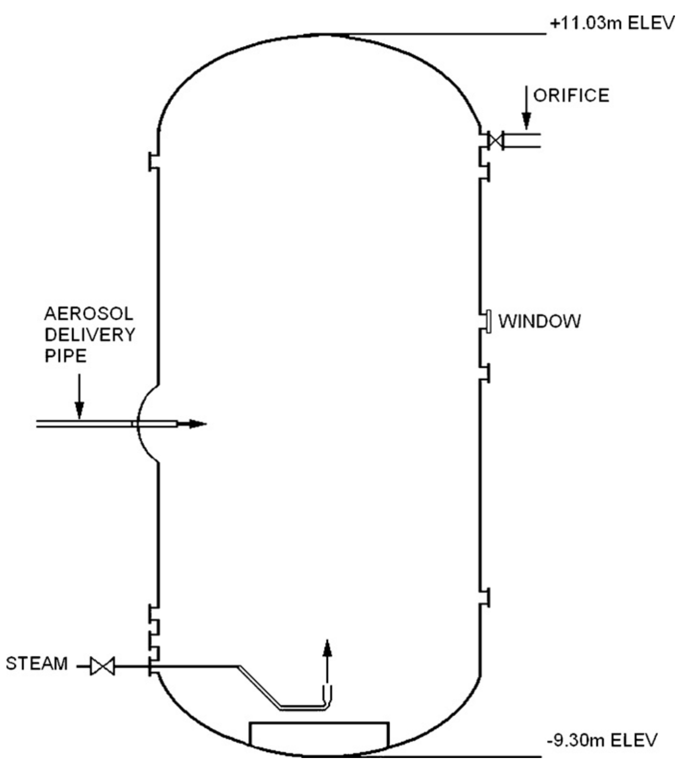

Fig. 6. Schematic view of LACE experimental facility.

injection rate of steam and hydrogen at high temperature together with aerosol injection, the scenario, though very improbable, provides an adequate containment transient to test the containment code capabilities. The ASTEC V1.3 code was assessed by comparing simulation results with those obtained with the MELCOR 1.8.5 code (Gauntt et al., 2000).

3. Models and main assumptions

3.1. Phebus FPT2 test

In the input model for the ASTEC code, the Phebus containment vessel was subdivided into three adequately selected control volumes ("zones") to discern the deposited aerosol masses on different surfaces (Herranz et al., 2006). The aerosol particle mass entering the containment was grouped in three aerosol components: iodine (I), cesium (Cs) and "mixture", the last including materials other than I and Cs. The total injected mass was 4.27×10^{-2} kg (Zabiego and Girard, 2004). The aerosol density was approximated from a mass-averaging over aerosol components. Aerosol particles were assumed to be spherical and distributed log-normally along the size domain. Preliminary size measurements from impactors suggested that aerosol size distributions are similar to those in the Phebus FPT1 test (Jacquemain et al., 2000). Thus, a mass median diameter of 1.11 μm was assumed with a geometric standard deviation of 1.9. Eventually, the aerodynamic mass mean diameter (AMMD) was estimated to be 2.8 μm. None of the aerosols was defined as hygroscopic. The large under-saturation state of the atmosphere allowed not to consider the water absorption by particles below saturation conditions (Herranz et al., 2006).

3.2. KAEVER experiments

The KAEVER vessel was modelled as a single zone. Aerosol parameters were prescribed in the input models based on data, provided by GRS (Firnhaber et al., 2002). The aerosol density of mixtures was approximated from a mass-averaging over aerosol components. The Kelvin effect ought to be considered only for soluble aerosols. However, as the ASTEC code does not allow separate modelling of the Kelvin effect for separate aerosol components, the experiments where both soluble and non-soluble aerosols were present were simulated without modelling the effect. The aerosol size range (diameters from 5×10^{-8} m to 1×10^{-4} m) was divided into 20 sections. Log-normal size distributions were prescribed. The mass median radii and the geometric standard deviations are shown in Table 1. The simulations were performed with version V1.2 of the code.

Table 1
Aerosol size parameters in simulations of KAEVER experiments.

Test	Mean mass radius (μm)	Geometric standard deviation
K148	0.996	0.336
K188	0.370	0.372
K186	0.567	0.182
K187	0.518	0.262

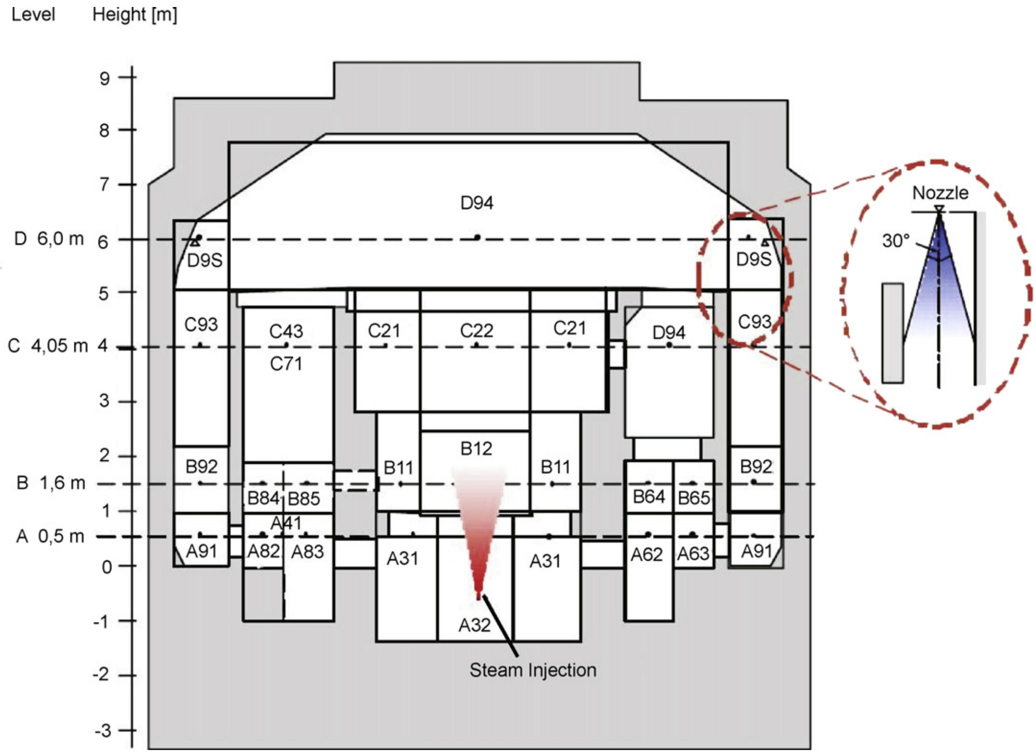

Fig. 7. Nodalisation of BMC for simulation of test sequence PACOS Px1.2.

3.3. PACOS Px1.2 experimental sequence

Simulations of the Px1.2 sequence with the ASTEC code were performed with two different nodalisations, both of them consisting of 23 zones (Fig. 7) (Dapper et al., 2006):

- a default nodalisation (AST1.2v1_DEF), in which the steam injection was simulated by prescribing adequate flow resistance coefficients in the steam injection area and overflow openings. The interaction between spray droplets and nearby walls was not modelled.
- an optimized nodalisation (AST1.2v1_OPT), with all flow resistance coefficients set to 1.0. The interaction between spray droplets and nearby walls was modelled.

The main parameter of the efficiency of a spray system is the falling distance of the droplets. The ASTEC spray model considers the evolution of the spray droplet size distribution with the height in the containment due to kinetic and thermal relaxation, gravitational coagulation and mass transfer with the surrounding gas. The thermal resistance inside the droplets is neglected, because the temperature difference between the liquid bulk and the droplet surface temperature makes no significant difference if the transfer to the droplet is considered. For the coalescence of the droplets, neither the droplet trajectories nor collisions at the spray ring outlet nor the interactions with vertical walls are considered explicitly. These phenomena are considered implicitly by the mass median diameter and the standard deviation of the initial droplet size distribution (Layly and Plumecocq, 2004).

3.4. LACE LA4 experiment

The LACE vessel was modelled as a single zone. Namely, the main purpose of the development of the ASTEC code is to use it for simulations of severe accidents in actual nuclear power plants. As the CPA module uses a lumped-parameter approach, each compartment in a multi-compartment containment would in principle be modelled as a single zone. As the volume of the LACE vessel is of the same order of magnitude as the volume of an actual NPP containment compartment, the modelling of the LACE vessel as a single zone is adequate to assess the code capability to simulate accidents in actual plants.

Aerosol parameters were prescribed in the input model as described in the LACE LA4 report (McCormack et al., 1987), or by prescribing commonly used generic options. The aerosol density was approximated from a mass-averaging over aerosol components. The prescribed aerosol injection mass flow rates were calculated in the report by combining mass balances and measurements from filter samplings.

As in some simulations of KAEVER experiments, the Kelvin effect was not considered. The aerosol size range (diameters from 5×10^{-8} m to 1×10^{-4} m) was divided into 20 sections. Log-normal size distributions were prescribed. The mass median radii and the geometric standard deviations are shown in Table 2.

The simulation was performed with version V1.2 of the code.

3.5. VVER-1000/320 ABH scenario

A relatively coarse nodalisation of the VVER-1000 containment was used with 6 control volumes (Fig. 8). Volume CV810 represents the reactor cavity, CV820 the lower rooms, CV830 the primary system compartments, CV840 the spent fuel storage pool and CV850 the containment dome. Volume CV851 is a shaft between the dome and the lower rooms. Volume CV999 is the auxiliary building used only in wall heat transfer modelling. The containment natural leak FL900 conservatively leads directly to the environment (volume CV990). Small rooms in the lower part of the actual containment were merged into fewer rooms in the model. The main recirculation sump located below the lower rooms was modelled as part of them. There are 56 heat structures altogether in the model.

In order to ensure a consistent comparison of the results, models for MELCOR and ASTEC codes were prepared with identical con-

Table 2
Aerosol size parameters in simulation of LACE LA4 experiment.

Time interval (s)	CsOH aerosols		MnO aerosols	
	Mass median radius (μm)	Geometrical standard deviation	Mass median radius (μm)	Geometrical standard deviation
0–1830	0.3478	1.81	–	–
1831–3030	0.5746	1.80	0.5185	1.70
3031–4812	–	–	0.3861	2.56

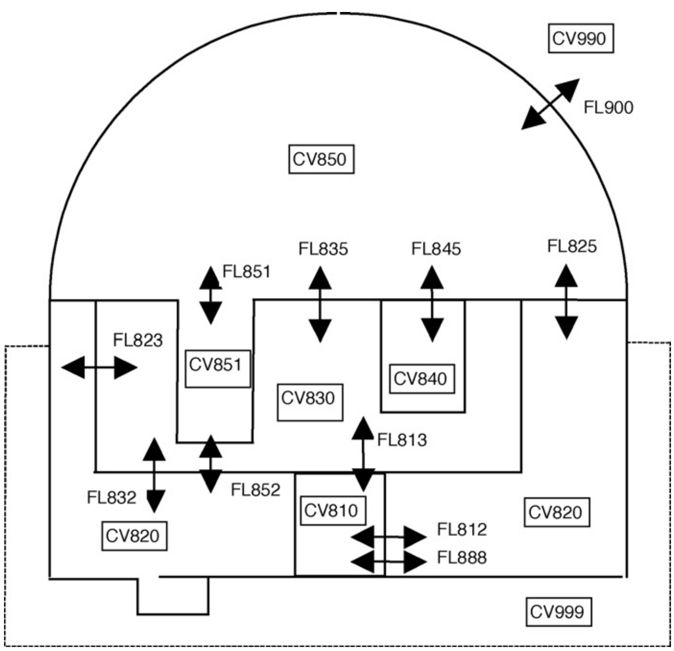

Fig. 8. Schematic view of VVER-1000/320 NPP containment nodalisation.

tainment data and initial conditions. A MELCOR "plant model" was used to generate the mass, energy and fission product sources from the primary system and the heat transfer through the primary and secondary system walls. MELCOR and ASTEC stand-alone "containment models" used these generated data as external sources.

In the simulations with the MELCOR code, 16 default fission product and material classes were defined and traced. Corresponding fission products were used in ASTEC. The decay heat linked with fission products was also transferred to the ASTEC input model. The mass median particle diameter 0.5 μm and standard deviation 1.6 were used in both MELCOR and ASTEC containment sources, taken from the MELCOR plant calculation for the period of prevailing fission product source.

4. Thermal-hydraulic results

4.1. Phebus FPT2 test

Fig. 9 shows the experimental and simulated atmosphere temperature in the Phebus.FP containment vessel during the test FPT2. Along with code results, three different experimental values are plotted. The one denoted as "Experiment" is the reported average temperature in the containment vessel, whereas TEPF840 and TEPF770 indicate local measurements of thermocouples located near dry and wet condenser parts, respectively. As may be observed, the ASTEC code estimates the atmosphere temperature quite accurately. Code deviations from the average experimental value are lower than 0.5 K, whereas local measurements can differ for more than 3 K.

At the beginning of the experiment "core degradation phase" (0–19,740 s), the variation of atmosphere energy depended essentially on energy input through steam injection and energy output by steam condensation. During the "core oxidation phase" (8520–9660 s), the input power was dominated by hydrogen injection, whereas the condensation output was much lower. During both phases, the nitrogen inlet flow could be neglected and the convective heat transfer was also relatively low.

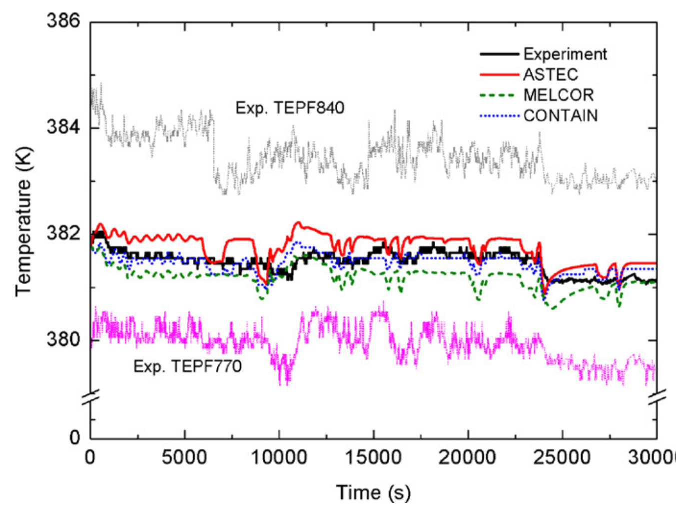

Fig. 9. Experimental and simulated temperature of Phebus containment vessel atmosphere during test FPT2.

Fig. 10 shows the measured and calculated pressure in the vessel. The simulation shows a similar evolution as the experimental measurements, but the calculated pressure is underestimated for up to 0.1 bar. This difference is associated with an underestimation of the steam partial pressure during the first 2000 s of the simulation. The deviations can be related to uncertainties of surface temperature in condensers, which governs the condensation and, as a consequence, the fraction of injected steam that remains air-

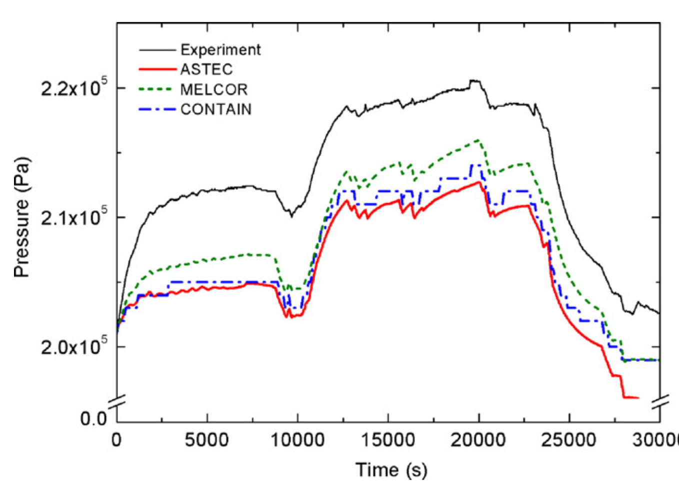

Fig. 10. Experimental and simulated pressure in Phebus containment vessel during test FPT2.

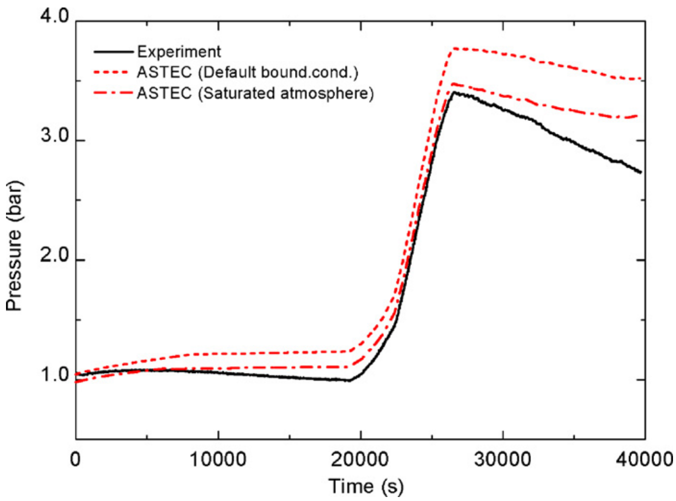

Fig. 11. Experimental and simulated pressure in KAEVER vessel during experiment K187.

borne (Herranz et al., 2007). Nevertheless, the discrepancy is still lower than 5% in absolute terms.

The test FPT2 was also simulated with the MELCOR 1.8.6 (Gauntt, 2005) and CONTAIN 2.0 (Murata et al., 1997) codes, using single-cell models of the containment vessel. Figs. 9 and 10 show that the results, obtained with these codes, do not exhibit large differences.

4.2. KAEVER experiments

For each considered KAEVER experiment, two simulations were performed: first with the enthalpy of injected steam, specified in the experiment descriptions ("default" boundary conditions), and then with a slightly increased enthalpy to actually simulate a saturated atmosphere (which supposedly occurred during the experiment and was not successfully simulated at first) – referred as "optimized" boundary conditions in the remaining part of the paper.

A good agreement between experimental and calculated thermal-hydraulic conditions was obtained in general with both default and optimized steam enthalpies. As illustrations, Figs. 11 and 12 show, respectively, the measured and calculated pressure and atmosphere temperature during experiment K187. The uncertainty of experimental measurements is ±0.01 bar for the pressure and ±1.2 K for the temperature. Although discrepancies may be observed, the presented results show that the vessel atmosphere thermal-hydraulic behaviour was (in general) satisfactorily simulated. The pressure increase after t = 19,000 s was due to the additional injection of the aerosol carrier gas (nitrogen). The pressure ceased to increase and started to decrease slowly (mainly due to steam condensation on the vessel walls) after the carrier gas injection was stopped at about t = 26,500 s. The qualitative agreement between the experimental and simulation pressure is good, although the calculated pressure increase caused by carrier gas injection is too high when default injection enthalpy was prescribed, and the further pressure decrease rate is not steep enough if a saturated atmosphere is simulated. This points to possible deficiencies in the modelling of steam condensation.

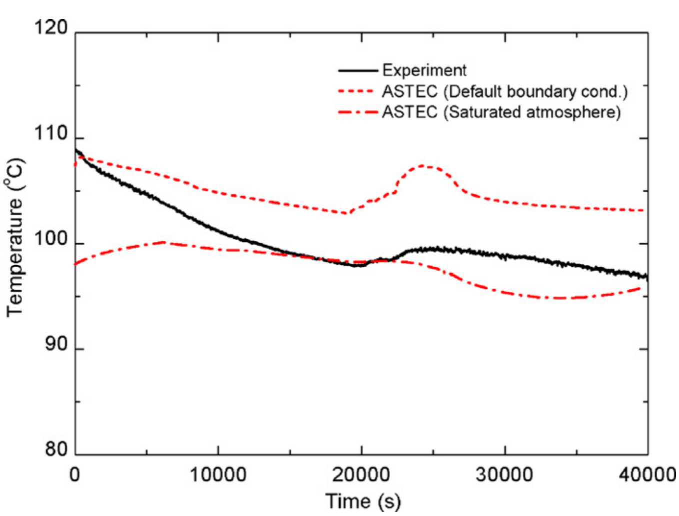

Fig. 12. Experimental and simulated atmosphere temperature in KAEVER vessel during experiment K187.

4.3. PACOS Px1.2 experimental sequence

The measured and calculated pressure in the BMC facility during the PACOS Px1.2 sequence are presented in Fig. 13. A good qualitative agreement was obtained. As to the quantitative agreement, the largest differences between measured and calculated values (with the ASTEC code) are of the order of 0.1 bar. It is remarkable that during the last phase, the pressure calculated using the optimized nodalisation agrees much less with the measured value than the pressure, calculated with the default model. This could be caused by bulk condensation and an underestimation of the leakage through the porous concrete vessel walls. Fig. 14 shows the atmosphere temperature in the dome of the facility. A good qualitative agreement was obtained during the first three phases, but not during the last phase. During the first phase, the temperature in the ASTEC simulations decreased, but less than in the experiment. This caused differences between measured and calculated temperatures during the second and third phase of up to 15 K. The best agreement with experimental results was achieved with the optimized ASTEC nodalisation. After the increase of the steam injection rate (phases 2 and 3), the temperature was not only overestimated by both ASTEC simulations during phase 4, but the calculated temperature also remained nearly constant instead of adopting a decreasing trend. A conspicuous feature during the entire simulated transient is also the higher temperature obtained with the default ASTEC nodalisation compared to the optimized nodalisation. This is due to the prescribed flow resistance coefficients in the steam injection area. The simulation results in other zones are qualitatively and quantitatively in good agreement with the experiment.

The PACOS Px1.2 sequence was also simulated with the lumped-parameter code COCOSYS (Bendiab et al., 2004; Klein-Hessling et al., 2000). In order to ensure a consistent comparison of both codes, the COCOSYS nodalisation was identical to the ASTEC optimized nodalisation. As may be seen in Figs. 13 and 14, the largest difference between the ASTEC and COCOSYS simulations occurred during the last phase, where the temperature calculated with the COCOSYS code was the lowest. However, it still exhibited the same kind of qualitative discrepancy with the experimental results as the temperatures, calculated with the ASTEC code. The simulation results in other zones are also qualitatively and quantitatively in good agreement with the experiment.

4.4. LACE LA4 experiment

The simulation of the LACE LA4 experiment provided a good general agreement of calculated thermal-hydraulic variables with experimental results. Figs. 15 and 16 show, respectively, the pressure and atmosphere temperature during the experiment (both experimental measurements and simulation results). The uncertainty of experimental measurements is ±2% for the pressure and ±3% for the temperature. The steep increase of pressure and tem-

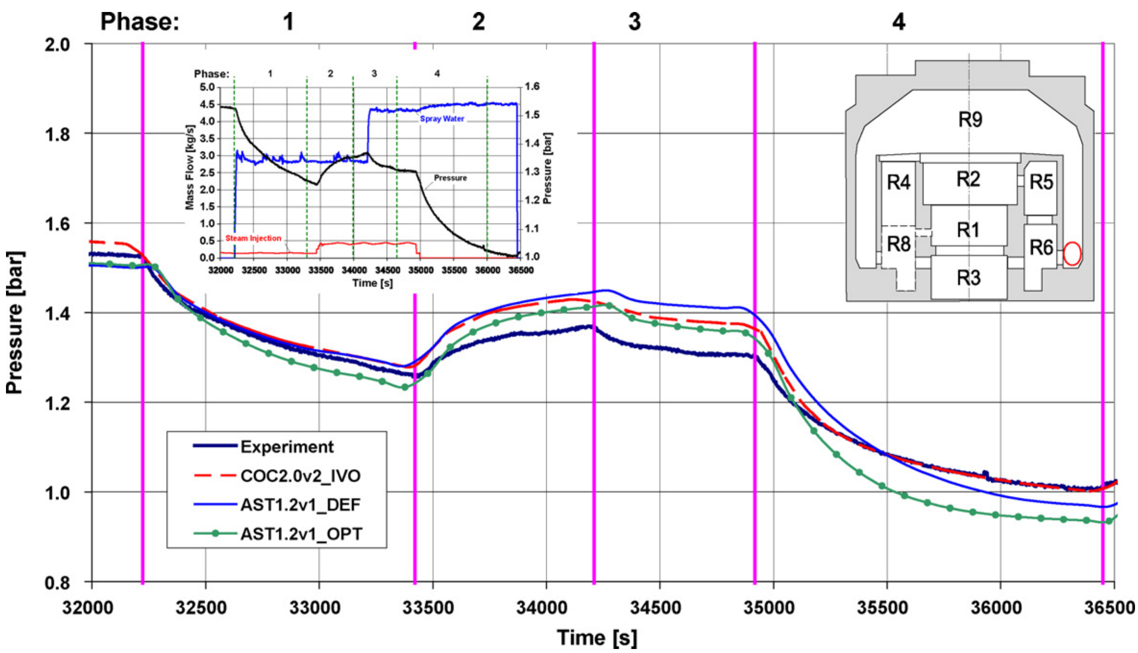

Fig. 13. Experimental and simulated pressure in BMC during PACOS Px1.2 sequence.

perature before $t = 0$ s was caused by the initial steam injection. After $t = 0$ s, steam injection was continued, but with a lower mass flow rate. The injection of the aerosol carrier gas (nitrogen) also contributed to the pressure increase. The steep pressure increase stopped after steam injection through the aerosol delivery line was discontinued (and steam was further injected only through the main line). This caused a period of "steady state" (phase 5 of the experiment). The venting, which started at about $t = 16,800$ s, caused a steep pressure and temperature decrease. Through all these phases, the agreement between experimental and simulated variables is very good. After the venting was stopped, both the pressure and the atmosphere temperature slightly increased before decreasing again, once the steam injection through the main line was stopped at about $t = 36,000$ s. During this phase, the discrepancies are higher, but still moderate. Another qualitative discrepancy is that, contrary to the experiment, the simulated atmosphere was not saturated until about $t = 18,000$ s. This seems to be a recurrent deficiency of the ASTEC code.

4.5. VVER-1000 ABH scenario

Some of the thermal-hydraulic variables during the simulated VVER scenario, calculated with the ASTEC and MELCOR codes, are shown in Figs. 17 and 18: Fig. 17 shows the calculated pressures, whereas Fig. 18 shows the atmosphere temperature in some compartments, as well as the pool temperature. The ASTEC code

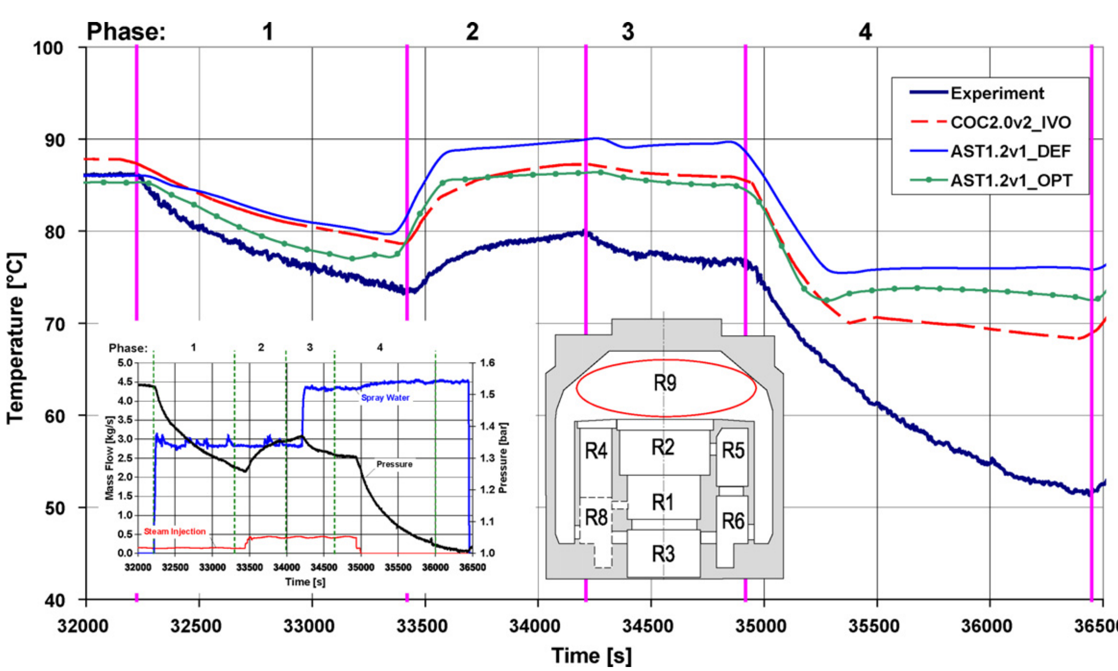

Fig. 14. Experimental and simulated temperature in BMC dome region during PACOS Px1.2 sequence.

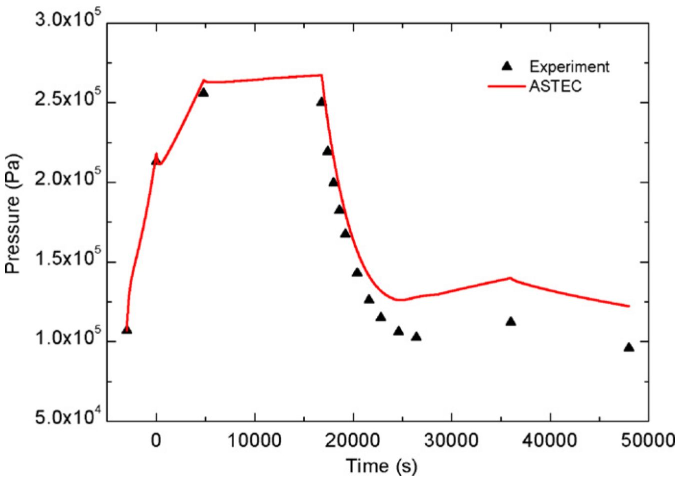

Fig. 15. Experimental and simulated pressure in LACE vessel during experiment LA4.

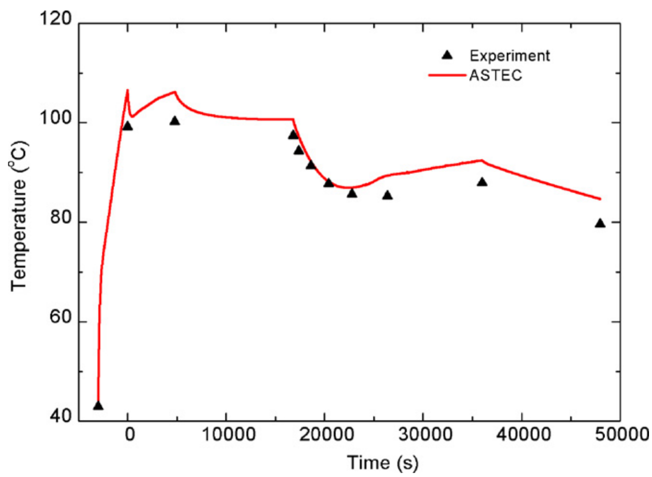

Fig. 16. Experimental and simulated atmosphere temperature in LACE vessel during experiment LA4.

calculated higher pressure and temperature, with the main difference occurring shortly after the blowdown phase in the first 15 min of the scenario. The differences tend to remain stable later and results from both codes follow the same pattern. The differences in

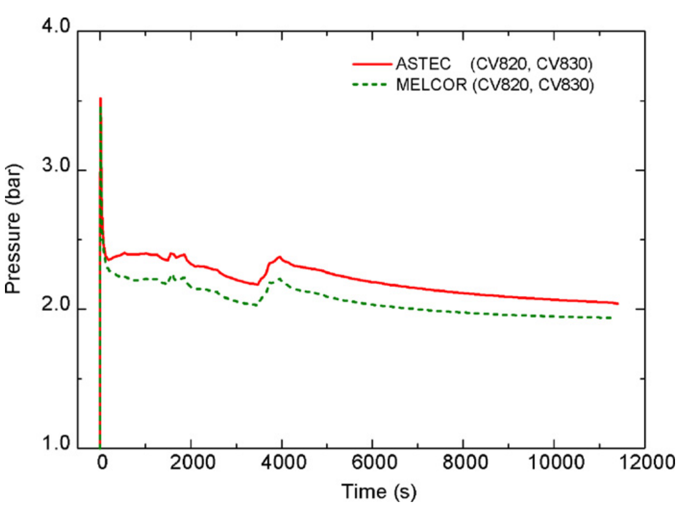

Fig. 17. Pressure in VVER-1000 containment, calculated with ASTEC and MELCOR codes, during ABH scenario.

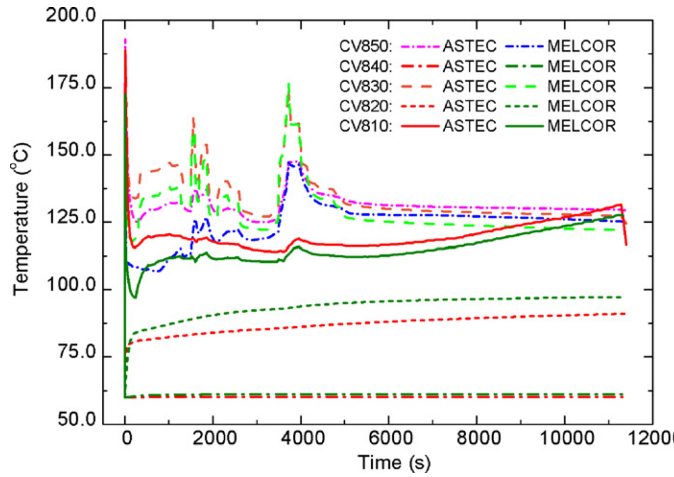

Fig. 18. Atmosphere and pool temperature in VVER-1000 containment, calculated with ASTEC and MELCOR codes, during ABH scenario.

atmosphere temperature in all volumes are similar to those of pressure, the temperature calculated with ASTEC being usually higher. The agreement between the trends calculated by both codes may also be observed on the rising cavity temperature later into the transient, caused by cavity heating by debris through the vessel wall. A very good agreement between codes was obtained for the blowdown pressure peak, 10 s after the accident initiation.

In general, the cooling of the atmosphere during the first minutes of the transient is more intense in the MELCOR simulation. This tendency changes later, when both simulations follow the same pattern. The origin of the differences was found in different heat transfer on the walls' surfaces, which was higher in the MELCOR simulation than in the ASTEC simulation during the first 10 min, and lower later. For instance, on the wall of the dome cylindrical compartment, condensation in the late phase of the MELCOR simulation reversed to film vaporization and the condensation heat flux became negative. The lower heat transfer calculated by the MELCOR code in the late phase may also be a consequence of the lower steam mole fraction and lower temperature.

A slightly different explanation of the differences is connected with energy transport to the sump. In Fig. 18, we may see a remarkable difference in the water temperature in the main sump. In the ASTEC simulation, this temperature is lower by about 8 K at the end of the sequence, although the difference in masses of water between the simulations is at most 1.1%. This means, that in the MELCOR simulation, more energy is stored in the sump and is therefore missing in the atmosphere. This may be explained by different heat transfer rates, especially during the water transfer to the sump.

5. Aerosol behaviour results

5.1. Phebus FPT2 experiment

Figs. 19 and 20 show the evolution of cesium and iodine airborne concentration in the Phebus containment vessel during the test FPT2. Data from gamma spectrometry and from filters are included. For both species, the simulation with the ASTEC code follows the experimental trend, although it slightly overestimates it. However, once the maximum concentration is reached, the code apparently speeds up the aerosol depletion with respect to the experiment. In the simulation, the main aerosol depletion mechanism was sedimentation on the vessel floor (Herranz et al., 2007). The airborne concentration calculated by the ASTEC code also decreases faster than the concentrations calculated by the MELCOR and CONTAIN codes. This behaviour is explained by the evolution of deposited

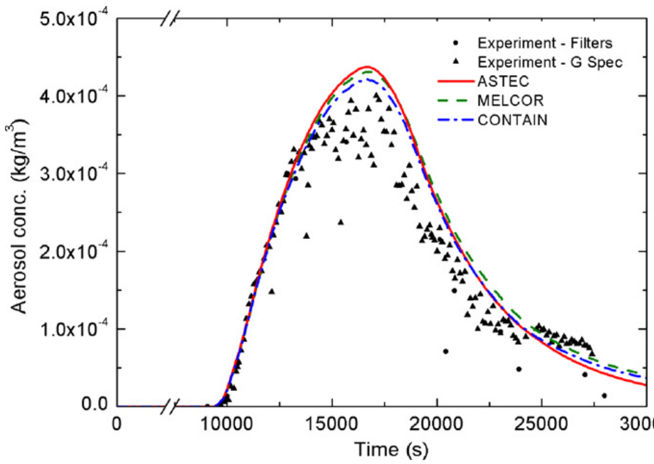

Fig. 19. Experimental and simulated cesium airborne concentration in Phebus containment vessel during test FPT2.

aerosol mass, which is slightly higher in the ASTEC simulation than in the simulations by the two other codes.

5.2. KAEVER experiments

For each simulated KAEVER experiment, calculated aerosol dry concentrations and aerosol wet concentrations in the vessel atmosphere were compared to experimental measurements. In general, maximum values of calculated dry aerosol concentrations agree well with the measured values (as an example, Fig. 21 shows experimental and simulation results for experiment K187; in this experiment, aerosol injection ended at time 26,400 s; the uncertainty of aerosol concentration measurements was not reported in available documents, neither for dry nor for wet aerosol concentration). When saturation conditions were adequately simulated with optimized enthalpies, the calculated dry aerosol concentration decreased faster than the experimental value (except for experiment K188, where the agreement was very good). In the simulation of experiment K187, although the calculated rate of decrease agrees better with the experiment if the atmosphere saturation is not adequately simulated (with default enthalpies), this would cause the airborne concentration to be overestimated on a longer time interval. The timing of the increase and the maximum value of wet aerosol concentration agree well with experimental data, provided that the atmosphere saturation is adequately reproduced (Fig. 22 shows experimental and simulation results for experiment

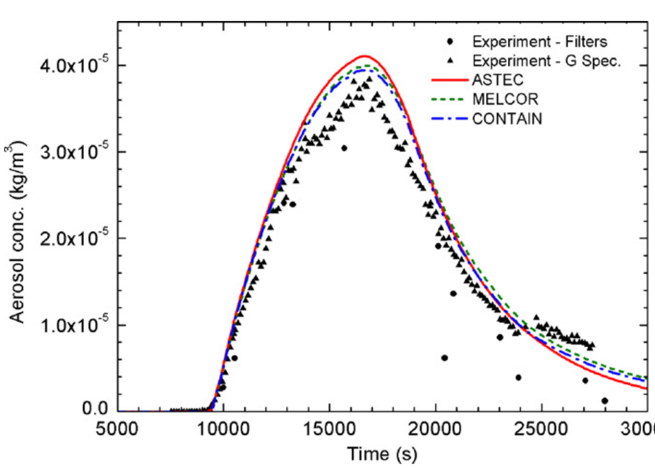

Fig. 20. Experimental and simulated iodine airborne concentration in Phebus containment vessel during test FPT2.

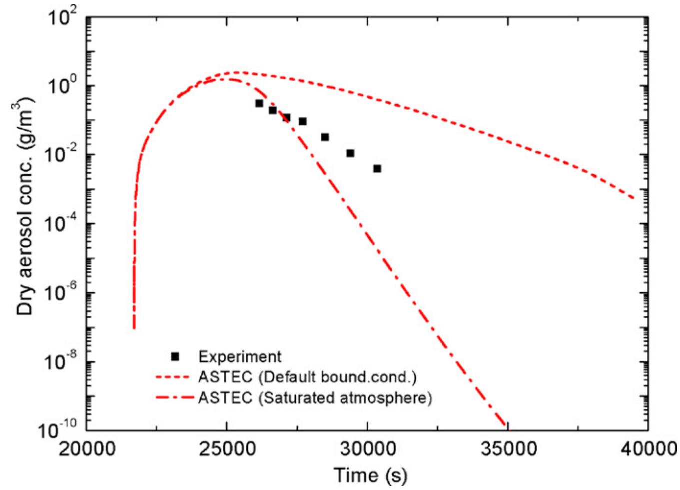

Fig. 21. Experimental and simulated dry aerosol concentration in KAEVER vessel atmosphere during experiment K187.

K187). However, in comparison to experimental data, the subsequent concentration decrease is much too slow, so that the aerosol wet concentration in the vessel atmosphere is overestimated. Nevertheless, the results show the importance of correctly simulating the atmosphere saturation. Also, as the modelling of aerosol mixtures is inherently simplified (for instance, no separate treatment of Kelvin effect solely for soluble components, and single prescribed value for aerosol density), these simulations should sometimes be seen mostly as a mean to obtain indicative values.

5.3. LACE LA4 experiment

The experimental and simulated dry aerosol mass concentrations of soluble (CsOH) and non-soluble (MnO) aerosols in the atmosphere of the LACE test vessel during experiment LA4 are shown in Fig. 23. The uncertainty of the experimental measurements is ±20%. The simulated concentration of non-soluble MnO aerosols agrees very well with the experimental results. The simulated behaviour of soluble CsOH aerosols was similar, which could have been expected as the ASTEC code does not allow different values of some important parameters for separate aerosol components (see remarks in discussion of KAEVER results). However, during the experiment, soluble aerosols behaved differently from non-soluble

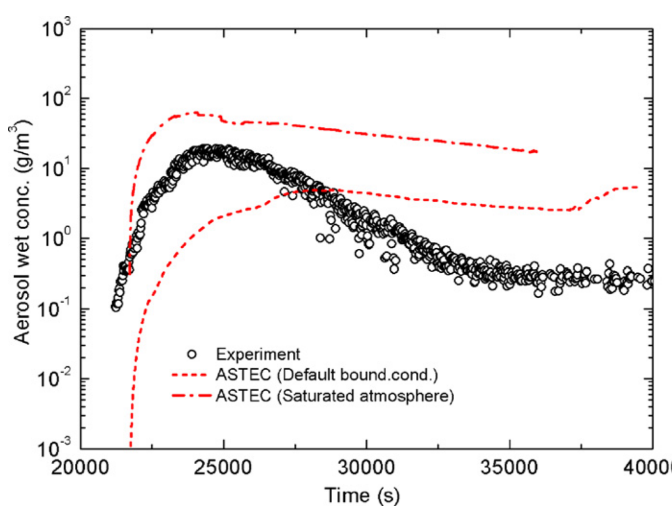

Fig. 22. Experimental and simulated wet aerosol concentration in KAEVER vessel atmosphere during experiment K187.

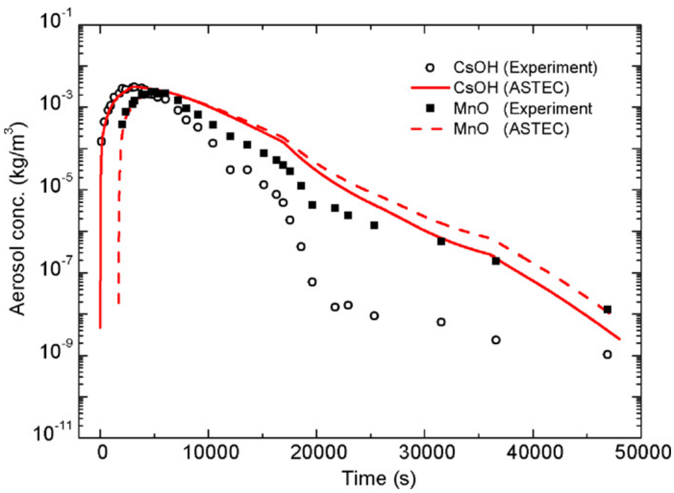

Fig. 23. Experimental and simulated dry aerosol concentration in LACE vessel atmosphere during experiment LA4.

ones (aerosol depletion occurred much faster). Thus, the simulated pattern of CsOH aerosol concentration decrease is different from the experimental one, although corresponding maximum and final values agree well with measured values. This discrepancy between patterns could also be due to the low simulated atmosphere saturation in the early phases of the experiment. Nevertheless, the simulation with the ASTEC code still provides a sensible indication of the aerosol behaviour.

5.4. VVER-1000 ABH scenario

Fig. 24 shows the aerosol mass in the VVER-1000 containment atmosphere, calculated with ASTEC and MELCOR codes, during the simulated ABH scenario. The high aerosol concentration peak that may be observed in the MELCOR results at the beginning of the simulation (before the fission product release) represents fog.

The agreement is less satisfactory during the fission product aerosol deposition phase than in the initial phases of the transient. This can be explained by the differences in aerosol modelling, but also by slightly different thermal-hydraulic conditions when approaching the steam saturation and differences in wall surface heat transfer. The main difference in aerosol modelling is in the Brownian deposition. While the MELCOR code uses a standard

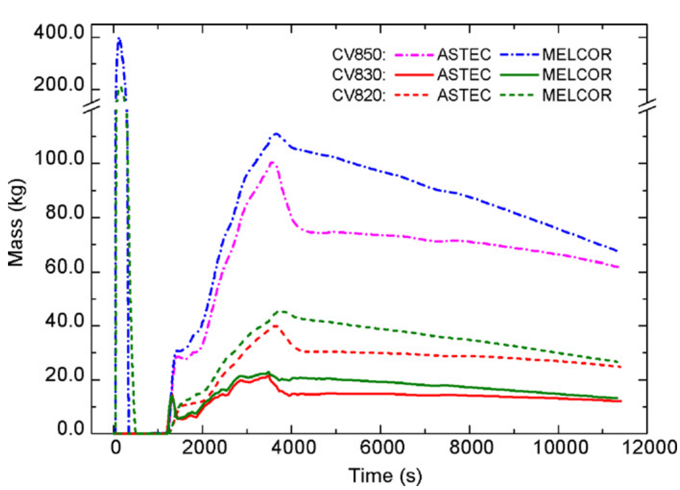

Fig. 24. Aerosol mass in VVER-1000 containment atmosphere, calculated with ASTEC and MELCOR codes, during ABH scenario.

model based on the Taylor–Prandtl hypothesis of stopping the turbulent diffusivity in the viscous boundary layer, in ASTEC a new model has been introduced in the CPA module (in version V1.2) based on the Landau and Lewich hypothesis of progressive damping of the diffusivity in the viscous layer (Layly and Plumecocq, 2006). The standard model leads to deposition proportional to $1/r$, where r is the particle radius and is efficient for nano-particles only. The new model follows the $r^{-2/3}$ rule and leads to deposition of a broader spectrum of particles. Indeed, about twice higher wall deposits on the dome part vertical walls were observed in the ASTEC than in the MELCOR simulation results. The ASTEC model also provided a relatively good explanation of the aerosol deposits on the cylindrical containment wall during Phebus FPT1 and FPT2 experiments.

6. Conclusions

Several experiments in facilities of different scales and a hypothetical scenario in a NPP containment were simulated with the ASTEC code to assess the modelling of thermal-hydraulic phenomena and aerosol behaviour in containments at accident conditions. Given the range of scales and of phenomena involved, the purpose of the work was to provide an overall assessment of the code capabilities.

Concerning thermal-hydraulic phenomena, ASTEC provides good estimations: taking into account experimental uncertainties, a good agreement has been found both qualitatively and quantitatively between simulation results and experimental data. In addition, when compared to other integral and/or system codes, ASTEC estimates were shown to be consistent.

Concerning aerosol behaviour, dry aerosol concentrations in vessels are in general well simulated, in small-, large- and real-scale systems. Minor deficiencies that were identified (in small-scale facilities) are slight overestimation of aerosol sedimentation and low deposition rate of wet aerosols. These features may be due to the influence of calculated thermal-hydraulic conditions or to inherent deficiencies of the models. The discrepancies are still within acceptable limits, so that the code may be used for safety analyses of actual plants. One of the features which could be implemented in the code would be the separate treatment of different aerosol components (such as prescription of aerosol density and modelling of Kelvin effect). On the other hand, the behaviour of aerosols in the containment atmosphere is inherently different from pressure and temperature equalisation, and also strongly depends on their injection location. Thus, a universally good agreement between experimental and simulation results, such as is obtained for thermal-hydraulic variables, may perhaps never be achieved with a lumped-parameter description. So, the ASTEC containment part, using a lumped-parameter approach, describes aerosol behaviour with enough accuracy by providing a reasonable evolution of airborne aerosol concentration along time and by resulting in an aerosol mass distribution at the end of simulation that looks consistent with experimental data. This does not exclude the possibility that some acting phenomena are missing in such lumped-parameter codes, but that either those phenomena are not dominant or that they would not change neither the evolution nor the final distribution to such an extent as to make its absence relevant.

Acknowledgments

The benefit from the European Commission RTD Programme for research is acknowledged.

The research performed by the Jožef Stefan Institute was partially financed by the Slovenian Research Agency under the research programme Reactor Engineering (P2-0026).

The PACOS experiments were operated by Battelle Ingenieurtechnik (now Becker Technologies GmbH) on behalf of the German Federal Ministry of Education, Science, Research and Technology (BMBF) under the contract number BMBF 15NU0962.

The COCOSYS validation on the PACOS experiment was sponsored by the German Federal Ministry of Economics and Technologies (BMWi) under the contract number BMWi 1501242.

The CIEMAT contribution was partially supported by the Spanish Nuclear Regulatory Authority (CSN).

The authors also acknowledge the help and support of the ASTEC maintenance team, and in one case the support from Wolfgang Luther (GRS). Many thanks also to the leader of the SARNET ASTEC topic Jean-Pierre van Dorsselaere (IRSN) for his valuable comments.

References

Bendiab, M., Fischer, K., Unger, H., Wagner, H.-J., Koch, M.K., 2004. Simulation des Thermohydraulik-Versuchs PACOS Px1.2 mit dem Containment-Analysecode COCOSYS. Technical Report, Lehrstuhl für Energiesysteme und Energiewirtschaft (LEE) – Ruhr-Universität Bochum, Germany (in German).

Bestele, J., Klein-Hessling, W., 2000. Containment thermal-hydraulics and aerosol and fission product behaviour. User guidelines. GRS Technical Note ASTEC-V0/DOC/00-14, Gesellschaft für Anlagen- und Reaktorsicherheit (GRS)mbH, Germany.

Dapper, M., Bendiab, M., Koch, M.K., 2006. Containment part of ASTEC validation on spray experiment PACOS Px1.2. Technical Report ASTEC-P63, SARNET, EC FI6O-CT-2004-509065, Lehrstuhl für Energiesysteme und Energiewirtschaft (LEE) – Ruhr-Universität Bochum, Germany.

Firnhaber, M., Fischer, K., Schwarz, S., Weber, G., 2002. ISP-44 KAEVER – experiments on the behaviour of core-melt aerosols in a LWR containment. NEA/CSNI/R(2003)5, Gesellschaft für Anlagen- und Reaktorsicherheit (GRS)mbH, Germany.

Gauntt, R.O., Cole, R.K., Erickson, C.M., Gido, R.G., Gasser, R.D., Rodriguez, S.B., Young, M.F., 2000. MELCOR Version 1.8.5, vol. 1. Primer and Users' Guide, vol. 2. Reference Manuals, NUREG/CR-6119, SAND2000-2417. Sandia National Laboratories, Albuquerque, NM, USA.

Gauntt, R.O., September 2005. MELCOR Version 1.8.6, Reference Manuals, NUREG/GR-6119, SAND2005-5713. Sandia National Laboratories, Albuquerque, NM, USA.

Herranz, L.E., Fontanet, J., Vela-García, M., 2006. In-containment thermal-hydraulic and aerosol behaviour during severe accidents: analysis of the PHEBUS-FPT2 experiment. In: Proc. Int. Congress on Advanced Power Plants ICAPP'06, Reno, NV, USA.

Herranz, L.E., Vela-García, M., Fontanet, J., López del Prá, C., 2007. Experimental interpretation and code validation based on the PHEBUS-FP programme: lessons learnt from the analysis of the containment scenario of FPT1 and FPT2 tests. Nucl. Eng. Des. 237, 2210–2218.

IRSN, 2002. FPT2 preliminary report and associated data, OECD CSNI (Committee for the Safety of Nuclear Installations).

Jacquemain, D., Bordon, S., Braemaeker, A., Barrachin, M., 2000. FPT1 Final Report, IPSN/DRS/SA/PDF Report SA1/00, IP00/479, Institut de Radioprotection et de Sûreté Nucléaire, France.

Kanzleiter, T., Holzbauer, H., Fischer, K., 1996. HYJET/PACOS-Versuche im Modellcontainment. Abschlussbericht, BF-R40.075-01, Project No. 15NU0962, Battelle Ingenieurstechnik GmbH, Eschborn, Germany.

Klein-Hessling, W., Arndt, S., Weber, G., 2000. COCOSYS V 1.2 User Manual. Gesellschaft für Anlagen- und Reaktorsicherheit (GRS)mbH, GRS-P-3/2, Germany.

Klein-Hessling, W., Schwinges, B., 1998. ASTEC V0 CPA Module, Program Reference Manual, Rev.0. Report ASTEC-V0/DOC/01-34, Institut de Radioprotection et de Sûreté Nucléaire, France, and Gesellschaft für Anlagen- und Reaktorsicherheit (GRS)mbH, Germany.

Kljenak, I., Mavko, B., 2006a. Simulation of KAEVER experiments on aerosol behavior with the ASTEC CPA V1.2 code. Report IJS-DP-9291, Jožef Stefan Institute, Ljubljana, Slovenia.

Kljenak, I., Mavko, B., 2006b. Simulation of LACE LA4 experiment on aerosol behavior in a nuclear power plant containment with the ASTEC CPA V1.2 code. Report IJS-DP-9484, Jožef Stefan Institute, Ljubljana, Slovenia.

Kljenak, I., Mavko, B., 2007. Simulation of LACE LA4 experiment on aerosol behavior in a NPP containment at severe accident conditions with the ASTEC CPA code. In: Proc. 15th Int. Conf. on Nuclear Engineering, Nagoya, Japan.

Layly, V.D., Plumecocq, W., 2004. Emergency spray modelling in the ASTEC code description and qualification, Rev.0, ASTEC-V1/MEM/03-11. Note Technique DPAM/SEMIC 2004/31, Institut de Radioprotection et de Sûreté Nucléaire, France.

Layly, V.D., Plumecocq, W., 2006. Dépôts des aerosols sur les parois de l'enceinte PHEBUS. In: ASFERA – 22ème congrès français sur les aerosols, Paris, France.

McCormack, J.D., Hilliard, R.K., Salgado, J.M., 1987. Final report of experimental results of LACE test LA4 – late containment failure with overlapping aerosol injection periods, Westinghouse, USA.

Murata, K.K., Williams, D.C., Tills, J., Griffith, R.O., Gido, R.G., Tadios, E.L., Davis, F.J., Martinez, G.M., Washington, K.E., December 1997. Code Manual for CONTAIN 2.0: A Computer Code for Nuclear Reactor Containment Analysis. Sandia National Laboratories, Albuquerque, NM, USA.

Ritter, G., Zabiego, M., 2002. FPT2 preliminary report, IRSN IP/02/514. Institut de Radioprotection et de Sûreté Nucléaire, France.

Van Dorsselaere, J.P., Schwinges, B., 2006. Overview of the integral code ASTEC V1.3, DPAM/ASTEC 2006-362, GRS ASTEC 06/02. Institut de Radioprotection et de Sûreté Nucléaire, France, and Gesellschaft für Anlagen- und Reaktorsicherheit (GRS)mbH, Germany.

Wilkening, H., Baraldi, D., Heitsch, M., 2007. CFD simulations of light gas release and mixing in the Battelle Model Containment with CFX. Nucl. Eng. Des. 238, 618–626.

Zabiego, M., Girard, J.M., 2004. FPT2 – Analyses des résultats du dépouillement des mesures relatives aux filtres et impacters réalisées dans la cellule CECILE. Note Technique IRSN, Institut de Radioprotection et de Sûreté Nucléaire, France.